EUV and Soft X-Ray Optics

David Attwood
University of California, Berkeley

Cheiron School
September 2011
SPring-8

CheironSchool_Sept2011_Lec1.ppt 1

The short wavelength region of the electromagnetic spectrum

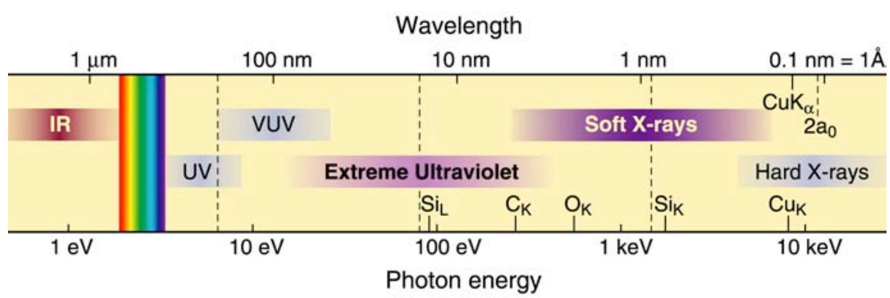

- See smaller features
- Write smaller patterns
- Elemental and chemical sensitivity

$$\hbar\omega \cdot \lambda = hc = 1239.842 \text{ eV nm}$$

$$n = 1 - \delta + i\beta \qquad \delta, \beta << 1$$

CheironSchool_Sept2011_Lec1.ppt 2

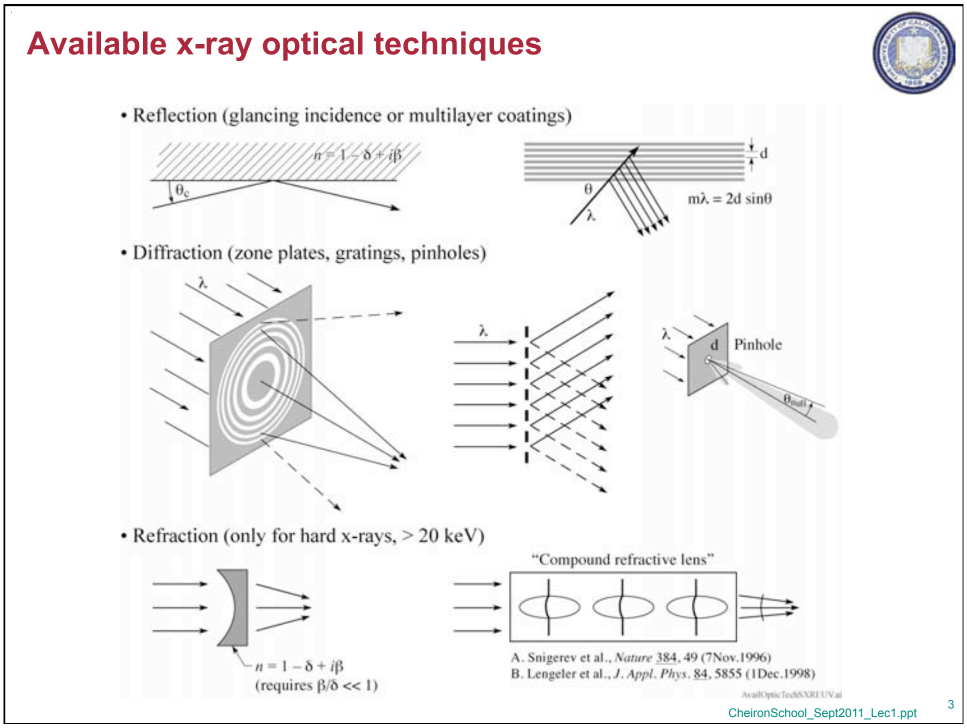
Available x-ray optical techniques
• Reflection (glancing incidence or multilayer coatings)
n = 1 – δ + iβ
θc
θ
λ
d
mλ = 2d sinθ
• Diffraction (zone plates, gratings, pinholes)
λ
λ
λ
d
Pinhole
• Refraction (only for hard x-rays, > 20 keV)
"Compound refractive lens"
n = 1 – δ + iβ
(requires β/δ << 1)
A. Snigerev et al., Nature 384, 49 (7Nov.1996)
B. Lengeler et al., J. Appl. Phys. 84, 5855 (1Dec.1998)
CheironSchool_Sept2011_Lec1.ppt
3

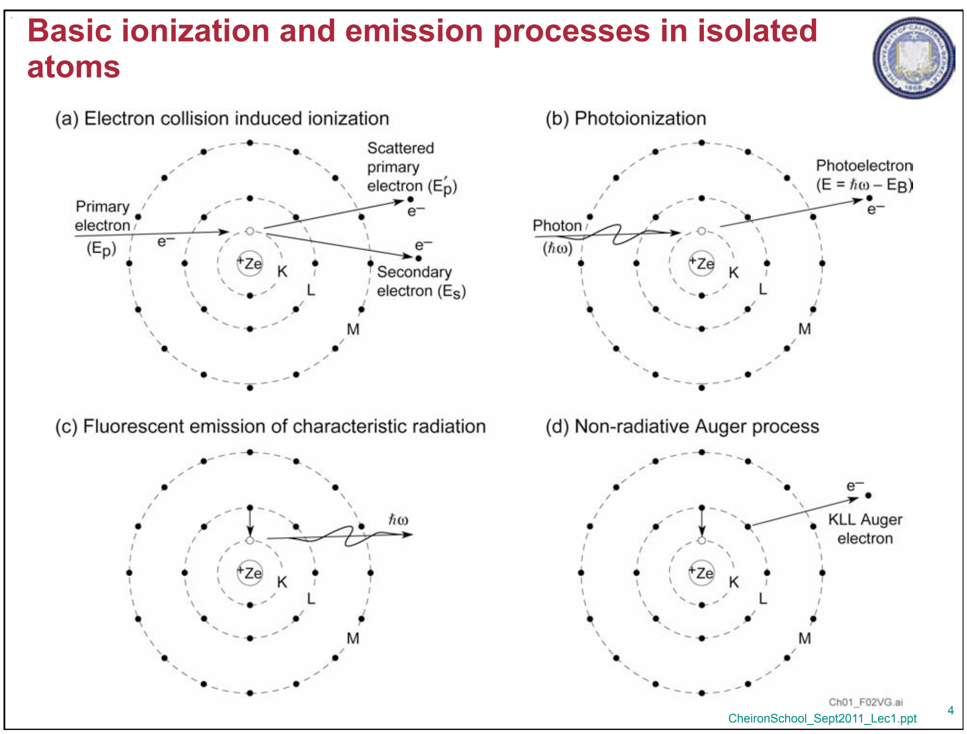
Basic ionization and emission processes in isolated atoms
(a) Electron collision induced ionization
Scattered primary electron (E′p)
Primary electron (Ep)
e−
e−
e−
Secondary electron (Es)
+Ze
K
L
M
(b) Photoionization
Photoelectron (E = ħω – EB)
Photon (ħω)
e−
+Ze
K
L
M
(c) Fluorescent emission of characteristic radiation
ħω
+Ze
K
L
M
(d) Non-radiative Auger process
e−
KLL Auger electron
+Ze
K
L
M
Ch01_F02VG.ai
CheironSchool_Sept2011_Lec1.ppt
4

Energy levels, absorption edges, and characteristic line emissions for a multi-electron atom

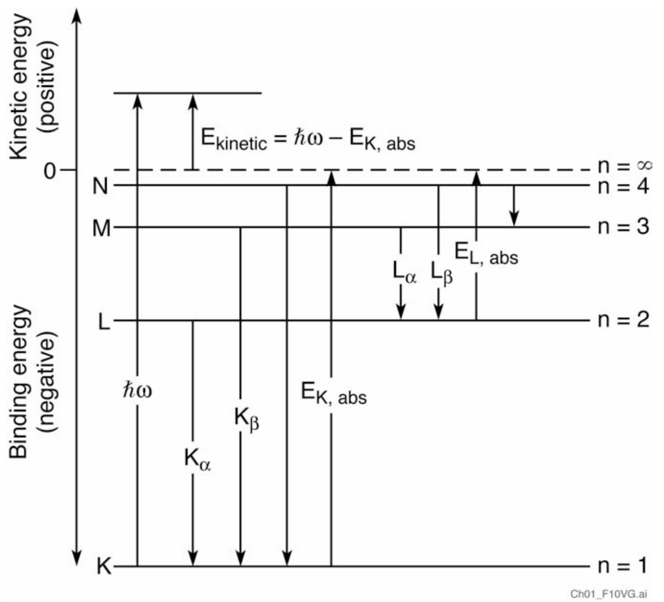

CheironSchool_Sept2011_Lec1.ppt 5

Energy levels, quantum numbers, and allowed transitions for the copper atom

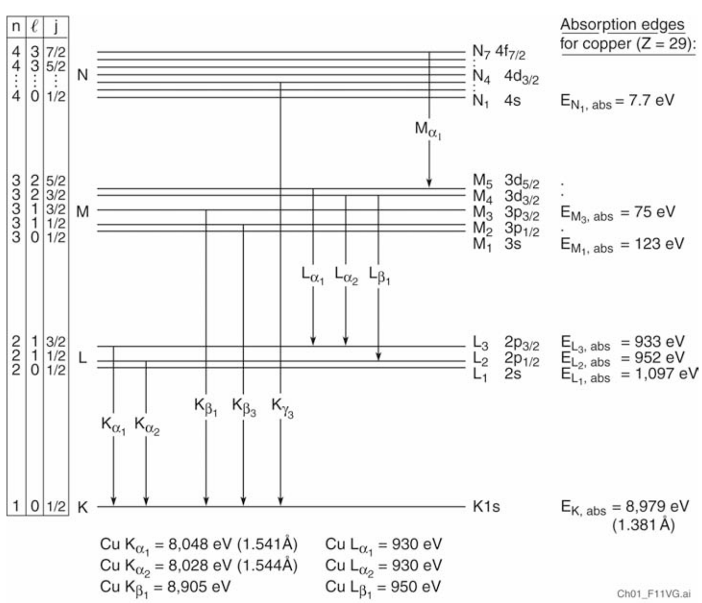

CheironSchool_Sept2011_Lec1.ppt 6

Refractive index from the IR to x-ray spectral region

$$\boxed{n(\omega) = 1 - \delta + i\beta} \quad (3.12)$$

$$\delta = \frac{n_a r_e \lambda^2}{2\pi} f_1^0(\omega) \quad (3.13a)$$

$$\beta = \frac{n_a r_e \lambda^2}{2\pi} f_2^0(\omega) \quad (3.13b)$$

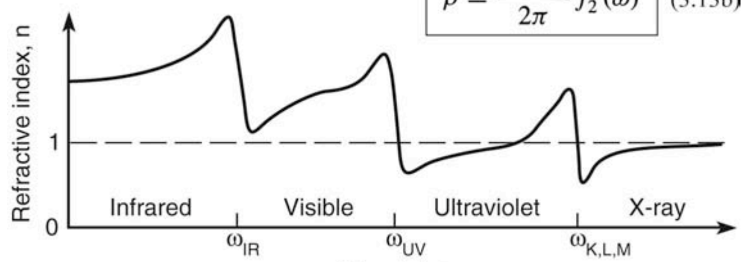

- λ^2 behavior
- δ & $\beta << 1$
- δ-crossover

Ch03_RefrcIndxIR.XR.ai

CheironSchool_Sept2011_Lec1.ppt 7

Refractive index at nanometer wavelengths

Refractive Index

$$n = 1 - \delta + i\beta = 1 - \frac{n_a r_e \lambda^2}{2\pi}(f_1^0 - if_2^0)$$

Atomic scattering factors

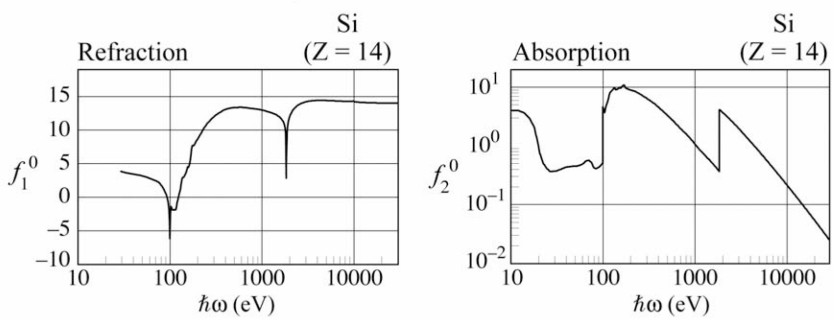

ScattrngRefracIndex_June2009.ai

CheironSchool_Sept2011_Lec1.ppt 8

Refractive index in the soft x-ray and EUV spectral region

$$n(\omega) = 1 - \frac{1}{2}\frac{e^2 n_a}{\epsilon_0 m} \sum_s \frac{g_s}{(\omega^2 - \omega_s^2) + i\gamma\omega} \qquad (3.8)$$

Noting that

$$r_e = \frac{e^2}{4\pi\epsilon_0 mc^2}$$

and that for forward scattering

$$f^0(\omega) = \sum_s \frac{g_s \omega^2}{\omega^2 - \omega_s^2 + i\gamma\omega}$$

where this has complex components

$$f^0(\omega) = f_1^0(\omega) - i f_2^0(\omega)$$

The refractive index can then be written as

$$\boxed{n(\omega) = 1 - \frac{n_a r_e \lambda^2}{2\pi}\left[f_1^0(\omega) - i f_2^0(\omega)\right]} \qquad (3.9)$$

which we write in the simplified form

$$\boxed{n(\omega) = 1 - \delta + i\beta} \qquad (3.12)$$

Ch03_RefracIndex2.ai

CheironSchool_Sept2011_Lec1.ppt 9

Photoionization and electron binding energies

TABLE B.1. Electron binding energies in electron volts for the elements in their natural forms.[a]

Element	K 1s	L_1 2s	L_2 $2p_{1/2}$	L_3 $2p_{3/2}$	M_1 3s	M_2 $3p_{1/2}$	M_3 $3p_{3/2}$	M_4 $3d_{3/2}$	M_5 $3d_{5/2}$	N_1 4s	N_2 $4p_{1/2}$	N_3 $4p_{3/2}$
1 H	13.6											
2 He	24.6[b]											
3 Li	54.7[b]											
4 Be	111.5[b]											
5 B	188[b]											
6 C	284.2[b]											
7 N	409.9[b]	37.3[b]										
8 O	543.1[b]	41.6[b]										
9 F	696.7[b]											
10 Ne	870.2[b]	48.5[b]	21.7[b]	21.6[b]								
11 Na	1070.8[c]	63.5[c]	30.4[c]	30.5[b]								
12 Mg	1303.0[c]	88.6[b]	49.6[c]	49.2[c]								
13 Al	1559.6	117.8[b]	72.9[b]	72.5[b]								
14 Si	1838.9	149.7[b]	99.8[b]	99.2[b]								
15 P	2145.5	189[b]	136[b]	135[b]								
16 S	2472	230.9[b]	163.6[b]	162.5[b]								
17 Cl	2822.4	270.2[b]	202[b]	200[b]								
18 Ar	3205.9[b]	326.3[b]	250.6[b]	248.4[b]	29.3[b]	15.9[b]	15.7[b]					
19 K	3608.4[b]	378.6[b]	297.3[b]	294.6[b]	34.8[b]	18.3[b]	18.3[b]					
20 Ca	4038.5[b]	438.4[c]	349.7[c]	346.2[c]	44.3[c]	25.4[c]	25.4[c]					
21 Sc	4492.8	498.0[b]	403.6[b]	398.7[b]	51.1[b]	28.3[b]	28.3[b]					
22 Ti	4966.4	560.9[c]	461.2[c]	453.8[c]	58.7[c]	32.6[c]	32.6[c]					
23 V	5465.1	626.7[c]	519.8[c]	512.1[c]	66.3[c]	37.2[c]	37.2[c]					
24 Cr	5989.2	695.7[c]	583.8[c]	574.1[c]	74.1[c]	42.2[c]	42.2[c]					
25 Mn	6539.0	769.1[c]	649.9[c]	638.7[c]	82.3[c]	47.2[c]	47.2[c]					
26 Fe	7112.0	844.6[c]	719.9[c]	706.8[c]	91.3[c]	52.7[c]	52.7[c]					
27 Co	7708.9	925.1[c]	793.3[c]	778.1[c]	101.0[c]	58.9[c]	58.9[c]					
28 Ni	8332.8	1008.6[c]	870.0[c]	852.7[c]	110.8[c]	68.0[c]	66.2[c]					
29 Cu	8978.9	1096.7[c]	952.3[c]	932.5[c]	122.5[c]	77.3[c]	75.1[c]					
30 Zn	9658.6	1196.2[b]	1044.9[b]	1021.8[b]	139.8[b]	91.4[b]	88.6[b]	10.2[b]	10.1[b]			

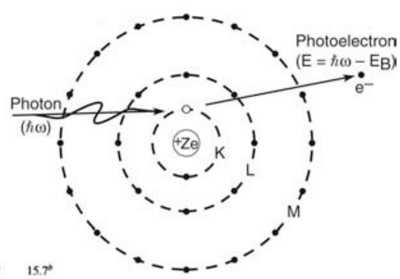

Ch01_ApB_T1rev2 & Photoionization.ai

CheironSchool_Sept2011_Lec1.ppt 10

Available x-ray optical techniques

• Reflection (glancing incidence or multilayer coatings)

• Diffraction (zone plates, gratings, pinholes)

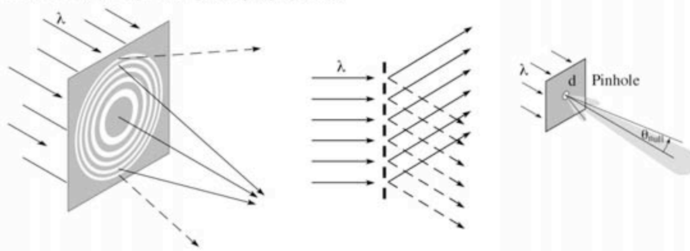

• Refraction (only for hard x-rays, > 20 keV)

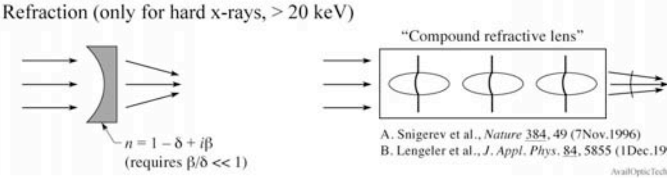

A. Snigerev et al., *Nature* 384, 49 (7Nov.1996)
B. Lengeler et al., *J. Appl. Phys.* 84, 5855 (1Dec.1998)

AvailOpticTechSXREUV.ai

Diffractive and reflective optics for EUV, soft x-rays and hard x-rays

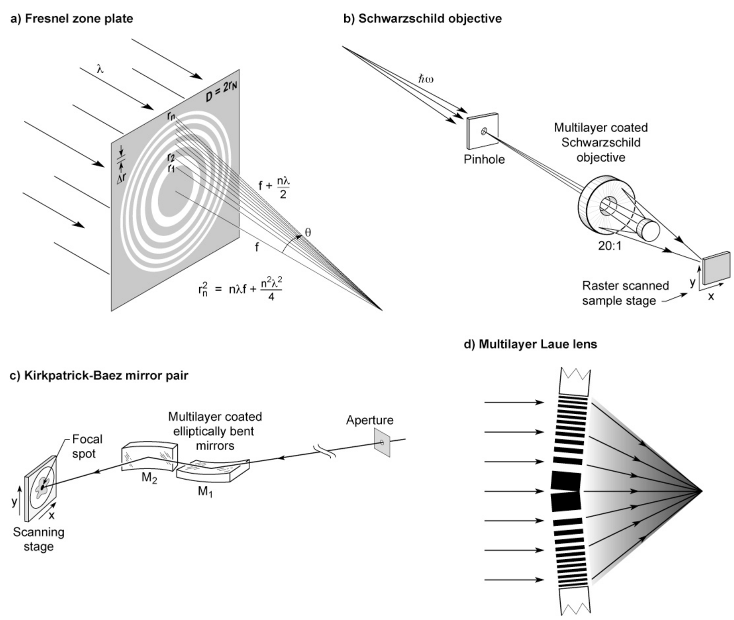

Professor David Attwood
Lecture 1, Sept. 28, 2011

Diffractive optics for soft x-rays and EUV

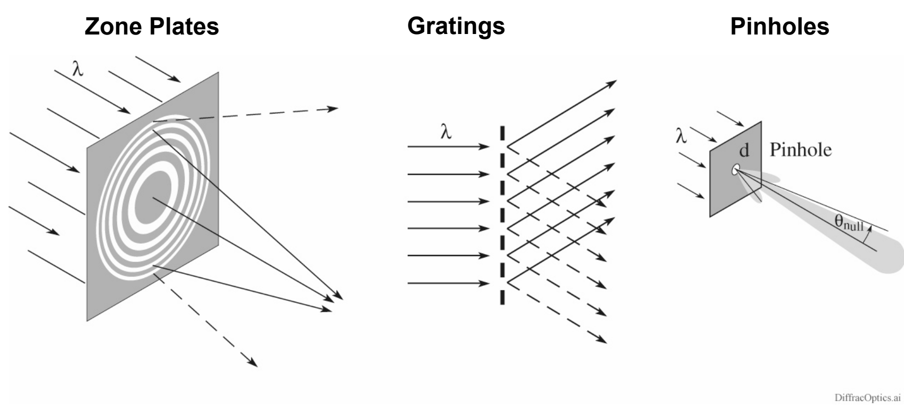

CheironSchool_Sept2011_Lec1.ppt 13

Diffraction from a transmission grating

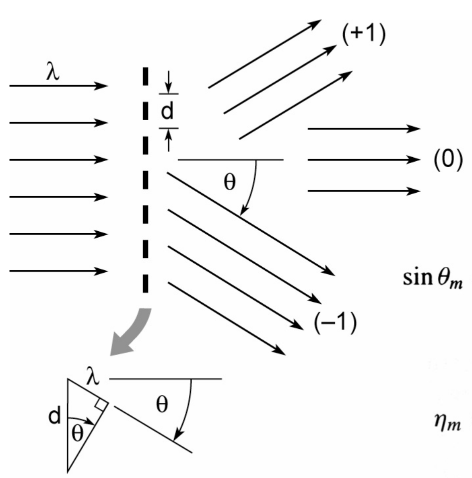

$$\sin\theta_m = \frac{m\lambda}{d}\,; \quad m = 0,\ \pm 1,\ \pm 2,\ \pm 3, \ldots \quad (9.2)$$

$$\eta_m = \begin{cases} \frac{1}{4} & m = 0 \\ 1/m^2\pi^2 & m \text{ odd} \\ 0 & m \text{ even} \end{cases} \quad (9.24)$$

(50% absorbed)

Ch09_F03VGrev.4.04.ai

CheironSchool_Sept2011_Lec1.ppt 14

A Fresnel zone plate lens

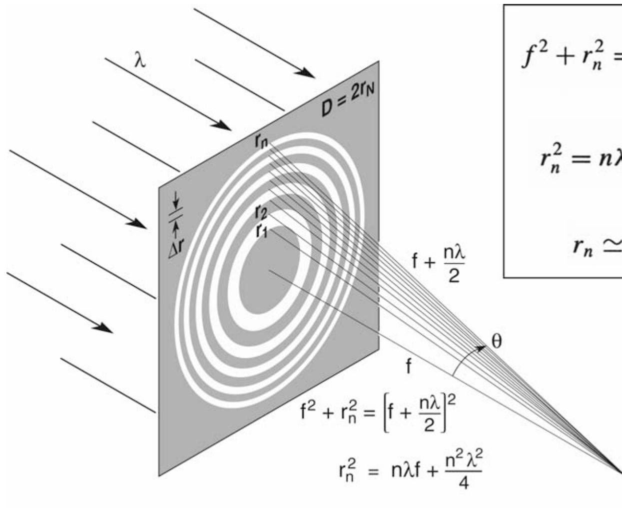

$$f^2 + r_n^2 = \left(f + \frac{n\lambda}{2}\right)^2 \quad (9.8)$$

$$r_n^2 = n\lambda f + \frac{n^2\lambda^2}{4} \quad (9.9)$$

$$r_n \simeq \sqrt{n\lambda f} \quad (9.10)$$

Ch09_F05VG.ai

CheironSchool_Sept2011_Lec1.ppt 15

A Fresnel zone plate lens used as a diffractive lens for point to point imaging

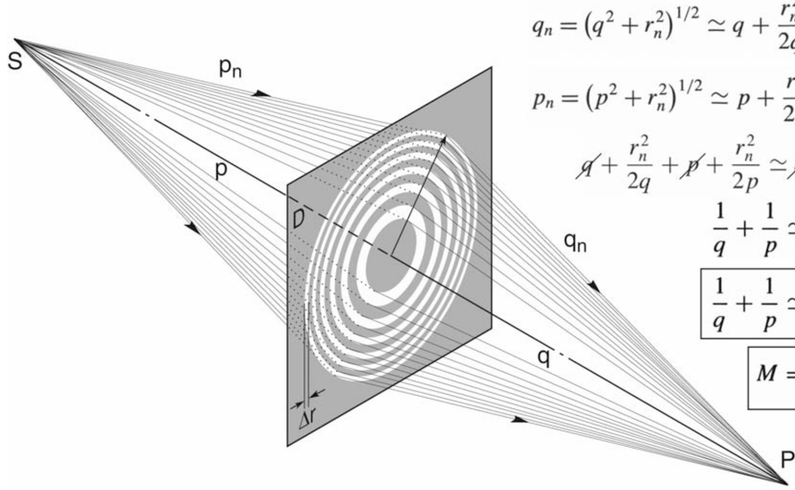

$$q_n + p_n = q + p + \frac{n\lambda}{2}$$

$$q_n = (q^2 + r_n^2)^{1/2} \simeq q + \frac{r_n^2}{2q}$$

$$p_n = (p^2 + r_n^2)^{1/2} \simeq p + \frac{r_n^2}{2p}$$

$$\cancel{q} + \frac{r_n^2}{2q} + \cancel{p} + \frac{r_n^2}{2p} \simeq \cancel{q} + \cancel{p} + \frac{n\lambda}{2}$$

$$\frac{1}{q} + \frac{1}{p} \simeq \frac{n\lambda}{r_n^2}$$

$$\boxed{\frac{1}{q} + \frac{1}{p} \simeq \frac{1}{f}} \quad (9.17)$$

$$\boxed{M = \frac{p}{q}} \quad (9.18)$$

Ch09_F02_modif.VG.ai

CheironSchool_Sept2011_Lec1.ppt 16

Depth of focus and spectral bandwidth

$$\Delta z = \pm \frac{1}{2} \frac{\lambda}{(\mathrm{NA})^2} \qquad (9.50)$$

$$\Delta z = \pm 2 \mathrm{F}^{\#2} \lambda = \pm 2 (\Delta r)^2 / \lambda \qquad (9.51)$$

$$\frac{\Delta \lambda}{\lambda} \leq \frac{1}{N} \qquad (9.52)$$

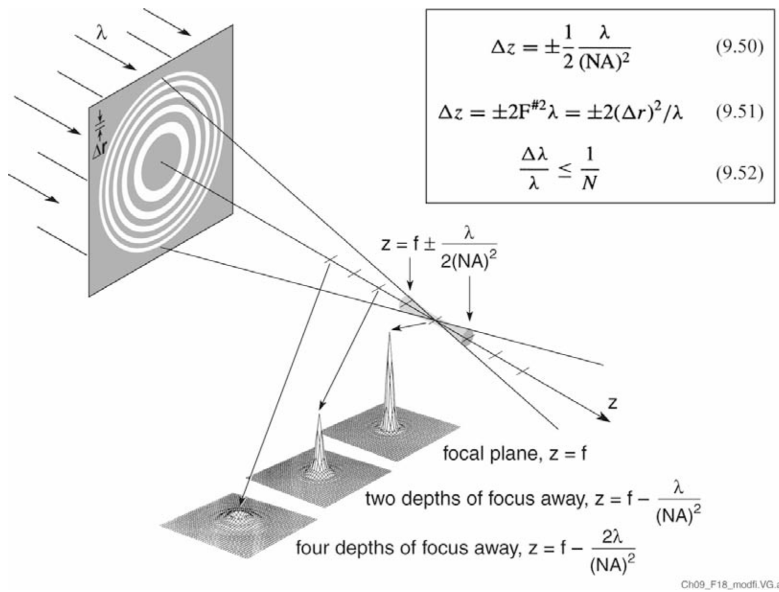

CheironSchool_Sept2011_Lec1.ppt 17

A Fresnel zone plate lens for soft x-ray microscopy

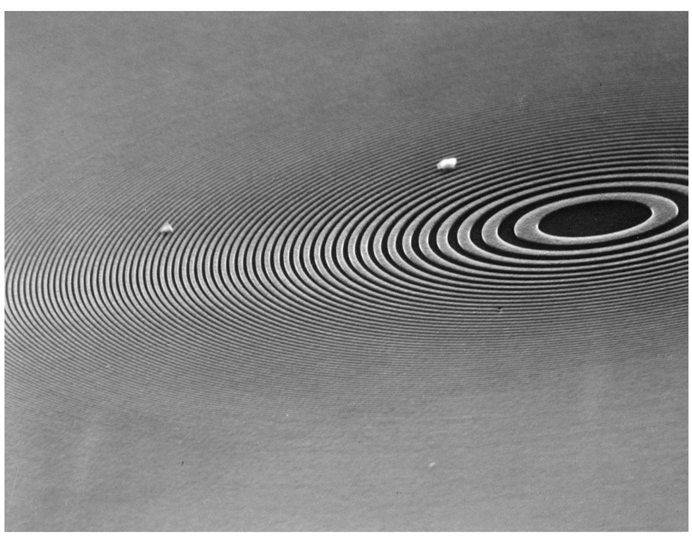

Courtesy of E. Anderson, LBNL

CheironSchool_Sept2011_Lec1.ppt 18

Zone plates for ALS STXM beamlines – "3D Engineered Nanostructures"

Δr = 35 nm, Δt = 180 nm Au, N = 1700
D = 240 µm, 3 x 95 µm^D central stop

Outer zone close-up

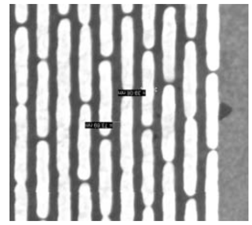

Inner zones

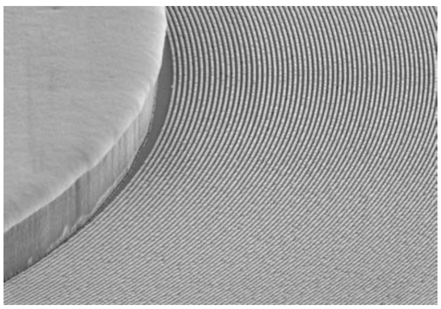

Outer zones

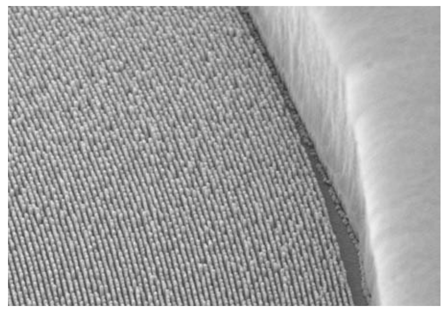

CheironSchool_Sept2011_Lec1.ppt 19

The Nanowriter: high resolution electron beam writing with high placement accuracy

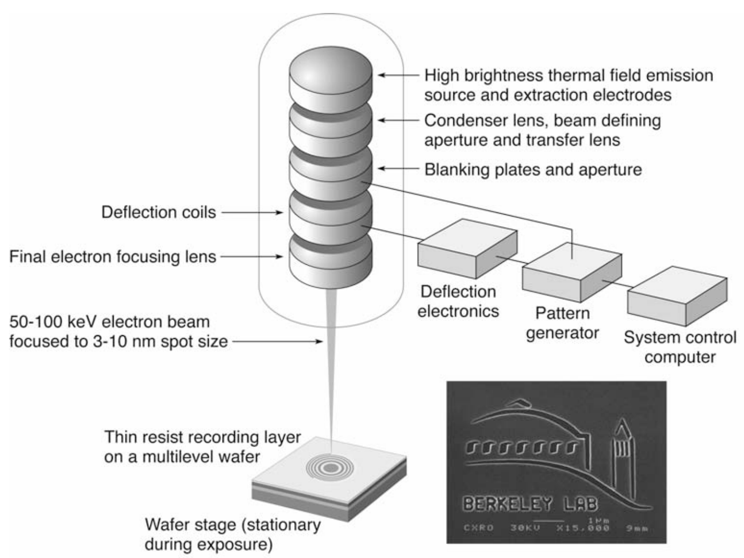

Courtesy of E. Anderson (LBNL)

CheironSchool_Sept2011_Lec1.ppt 20

Zones plates for soft x-ray image formation

Zone Plate Lens

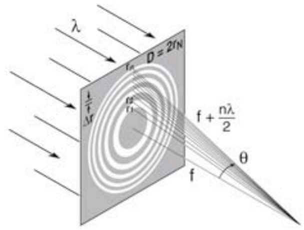

Soft X-Ray Microscope

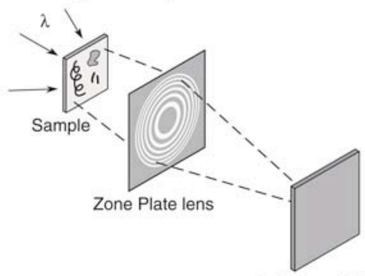

Zone Plate Formulae

$r_n^2 = n\lambda f + \frac{n^2\lambda^2}{4}$	(9.9)	$\lambda = 2.5$ nm, $\Delta r = 25$ nm, $N = 618$
$D = 4N\Delta r$	(9.13)	63 µm
$f = \frac{4N(\Delta r)^2}{\lambda}$	(9.14)	0.63 mm
$NA = \frac{\lambda}{2\Delta r}$	(9.15)	0.05
$\text{Res.} = k_1 \frac{\lambda}{\text{NA}} = 2k_1\Delta r$	$k_1 = 0.61$ ($\sigma = 0$)	$1.22\Delta r = 30$ nm
	$k_1 = 0.4$ ($\sigma = 0.45$)	$0.8\Delta r = 19$ nm
$\text{DOF} = \pm \frac{1}{2} \frac{\lambda}{(\text{NA})^2}$	(9.50)	1 µm
$\frac{\Delta\lambda}{\lambda} \le \frac{1}{N}$	(9.52)	1/700

CheironSchool_Sept2011_Lec1.ppt 21

New x-ray lenses: Improving contrast and resolution for x-ray microscopy

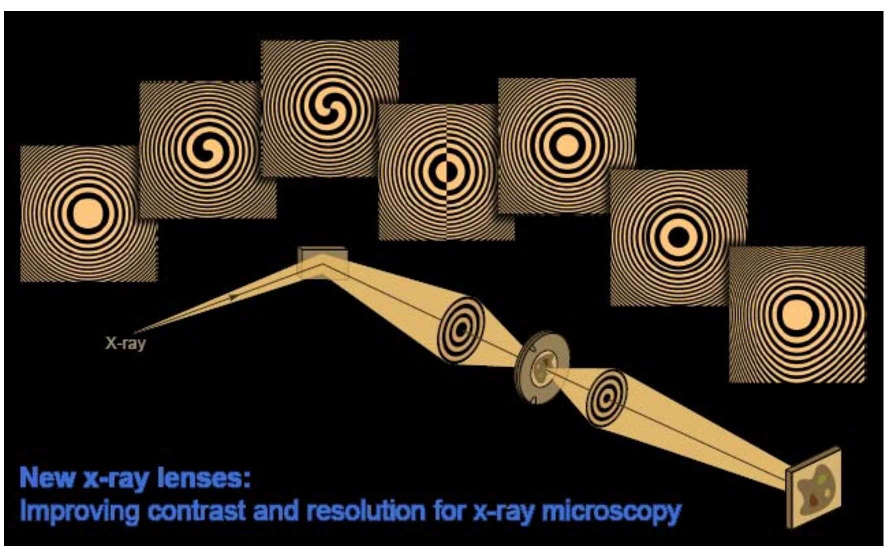

C. Chang, A. Sakdinawat, P.J. Fischer, E.H. Anderson, D.T. Attwood, Opt. Lett. 2006; Sakdinawat and Liu, Opt. Lett. 2007; Sakdinawat and Liu, Opt. Express 2008

CheironSchool_Sept2011_Lec1.ppt 22

Diffraction limited x-ray imaging

Diffraction limited imaging is limited by the finite wavelength and acceptance aperture:

$\Delta r_{resol.} = k_1 \lambda / NA$

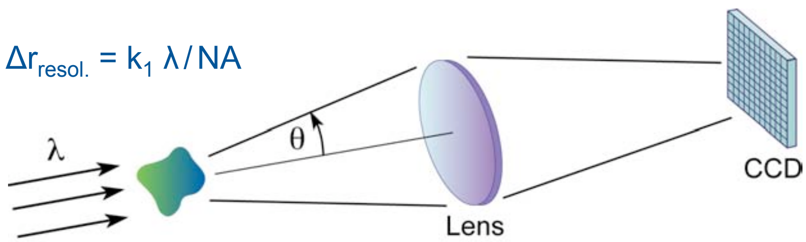

where $NA = n \sin\theta$ and the constant k_1 depends on illumination and specific image modulation criteria.
For x-rays

$$n = 1 - \delta + i\beta \qquad \delta, \beta << 1$$

CheironSchool_Sept2011_Lec1.ppt 23

Diffraction limited x-ray imaging

For example, the widely accepted Rayleigh criteria for resolving two adjacent, mutually incoherent, point sources of light, results in a 26% intensity modulation.

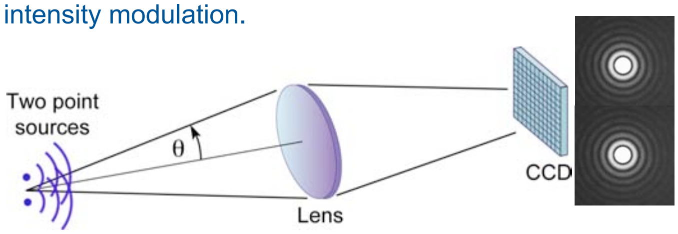

λ = 2.48 nm
(500 eV)

Two overlapping Airy patterns

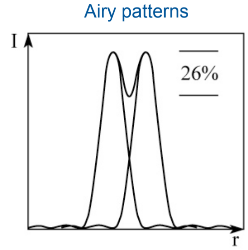

$\Delta r_{resol.} = 0.61 \lambda / NA$

Resultant intensity pattern when the two point sources are "just resolved", such that the central lobe maximum due to one point source overlaps the first minimum (dark ring) of the other.

Note: Other definitions are possible, depending on the application and the ability to discern separated objects.

CheironSchool_Sept2011_Lec1.ppt 24

Resolution and illumination

Achievable resolution can be improved by varying illumination:

An object pattern of periodicity d diffracts light and is just captured by the lens – setting the diffraction limited resolution limit.

Diffraction from an object of smaller periodicity, d/2, is just captured, and resolved, when illuminated from an angle.

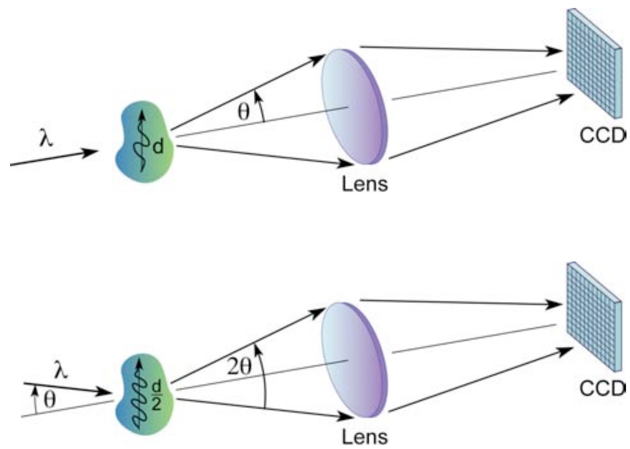

Resolution, illumination, and optical transfer function

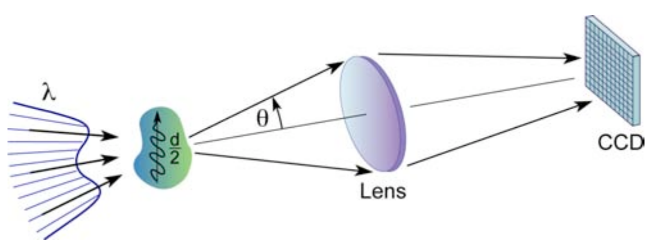

Spatial frequency response of the optical system can be optimized by tailoring the angular distribution of illumination.

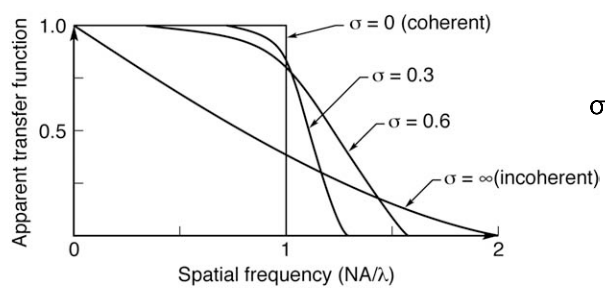

$$\sigma = \frac{NA_{cond}}{NA_{obj}} \qquad (10.3)$$

Nature Vol 435|30 June 2005|doi:10.1038/nature-3719

LETTERS

Soft X-ray microscopy at a spatial resolution better than 15 nm

Weilun Chao[1,2], Bruce D. Harteneck[1], J. Alexander Liddle[1], Erik H. Anderson[1] & David T. Attwood[1,2]

Analytical tools that have spatial resolution at the nanometre scale are indispensable for the life and physical sciences. It is desirable that these tools also permit elemental and chemical identification on a scale of 10 nm or less, with large penetration depths. A variety of techniques[1–7] in X-ray imaging are currently being developed that may provide these combined capabilities. Here we report the achievement of sub-15-nm spatial resolution with a soft X-ray microscope—and a clear path to below 10 nm—using an overlay technique for zone plate fabrication. The microscope covers a spectral range from a photon energy of 250 eV (~5 nm wavelength) to 1.8 keV (~0.7 nm), so that primary K and L atomic resonances of elements such as C, N, O, Al, Ti, Fe, Co and Ni can be probed. This X-ray microscopy technique is therefore suitable for a wide range of studies: biological imaging in the water window[8,9]; studies of wet environmental samples[10,11]; studies of magnetic nanostructures with both elemental and spin-orbit sensitivity[12–14]; studies that require viewing through thin windows, coatings or substrates (such as buried electronic devices in a silicon chip[15]); and three-dimensional imaging of cryogenically fixed biological cells[9,16].

The microscope XM-1 at the Advanced Light Source (ALS) in Berkeley[17] is schematically shown in Fig. 1. The microscope type is similar to that pioneered by the Göttingen/BESSY group (ref. 18, and references therein). A 'micro' zone plate (MZP) projects a full-field image to an X-ray-sensitive CCD (charge-coupled device), typically in one or a few seconds, often with several hundred images per day. The field of view is typically 10 μm, corresponding to a magnification of 2,500. The condenser zone plate (CZP), with a central stop, serves two purposes in that it provides partially coherent hollow-cone illumination[2], and, in combination with a pinhole, serves as the monochromator. Monochromatic radiation of $\lambda/\Delta\lambda = 500$ is used. Both zone plates are fabricated in-house, using electron beam lithography[19].

The spatial resolution of a zone plate based microscope is equal to $k_1\lambda/NA_{MZP}$, where λ is the wavelength, NA_{MZP} is the numerical aperture of the MZP, and k_1 is an illumination dependent constant, which ranges from 0.3 to 0.61. For a zone plate lens used at high magnification, $NA_{MZP} = \lambda/2\Delta r_{MZP}$, where Δr_{MZP} is the outermost (smallest) zone width of the MZP[20]. For the partially coherent illumination[21,22] used here, $k_1 \approx 0.4$ and thus the theoretical resolution is $0.8\Delta_{MZP}$, as calculated using the SPLAT computer program[23] (a two-dimensional scalar diffraction code, which evaluates partially coherent imaging). In previous results with a $\Delta r_{MZP} = 25$ nm zone plate, we reported[2] an unambiguous spatial resolution of 20 nm. Here we describe the use of an overlay nanofabrication technique that allows us to fabricate zone plates with finer outer zone widths, to $\Delta r_{MZP} = 15$ nm, and to achieve a spatial resolution of below 15 nm, with clear potential for further extension.

This technique overcomes nanofabrication limits due to electron beam broadening in high feature density patterning. Beam broadening results from electron scattering within the recording medium (resist), leading to a loss of image contrast and thus resolvability for

$\lambda = 1.52$ nm (815 eV)
$\Delta r = 15$ nm
$N = 500$
$D = 30$ μm
$f = 300$ μm
$\sigma = 0.38$
$0.8\,\Delta r = 12$ nm

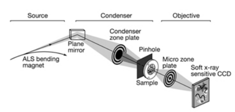

Figure 1 | A diagram of the soft X-ray microscope XM-1. The microscope uses a micro zone plate to project a full field image onto a CCD camera that is sensitive to soft X-rays. Partially coherent, hollow-cone illumination of the sample is provided by a condenser zone plate. A central stop and a pinhole provide monochromatization.

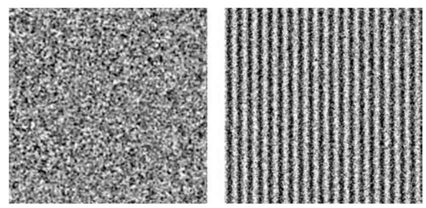

Figure 4 | Soft X-ray images of a 15.1 nm half-period test object, as formed with zone plates having outer zone widths of 25 nm and 15 nm.

Cr/Si test pattern (Cr L_3 @ 574 eV)
(2000 X 2000, 10^4 ph/pixel)

[1]Center for X-ray Optics, Lawrence Berkeley National Laboratory, 1 Cyclotron Road, MS 2-400, [2]Department of Electrical Engineerin California, Berkeley, California 94720, USA.

27

Hard x-ray imaging based on glancing incidence reflective optics

- Optics behave differently at these very short wavelengths (nanometers rather than 520 nm green light)
- The refractive index is less than unity, $n = 1 - \delta + i\beta$
- Waves bend away form the normal at an interface
- Absorption is significant in all materials and at all wavelength.
- Because of absorption, refractive lenses do not work, prisms do not, windows need to be extremely thin (100 nm or less).
- Because light is bent away from the surface normal, it possible to have "total external reflection" at glancing incidence – a commonly used technique.
- Kirkpatrick-Baez (KB) mirror pair

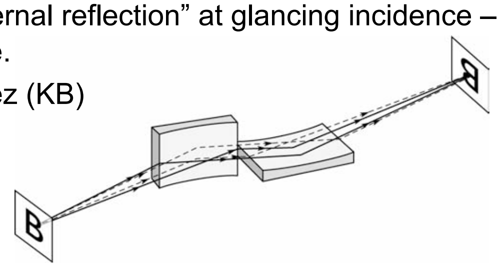

CheironSchool_Sept2011_Lec1.ppt 28

Glancing incidence optics

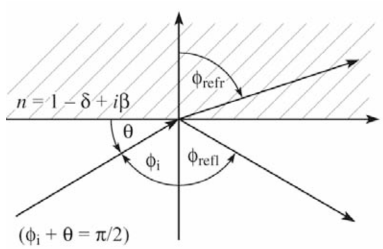

Snell's Law: $\boxed{\text{Sin } \phi_{refr.} = \frac{\text{Sin } \phi_i}{n}}$

Total external Reflection:

$$\phi_{refr.} \rightarrow \frac{\pi}{2} \text{ as } \phi_i \rightarrow \phi_{critical}$$

$$\text{Snell's Law: } 1 = \frac{\text{Sin } \phi_c}{1 - \delta}$$

$$\text{Sin}(90° - \theta_c) = 1 - \delta$$

$$\text{Cos } \theta_c = 1 - \delta$$

$$1 - \frac{\theta_c^2}{2} = 1 - \delta$$

$$\theta_c = \sqrt{2\delta}$$

For gold at 1 keV

$$\delta = 2.1 \times 10^{-3}$$

$$\theta_c = 3.7°$$

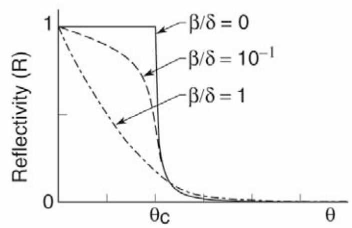

(www.cxro.LBL.gov ;
"X-ray properties of the elements"
"X-ray interaction with matter")

GlancngIncidncOptics.ai

CheironSchool_Sept2011_Lec1.ppt 29

Total external reflection with finite β

Glancing incidence reflection
as a function of β/δ

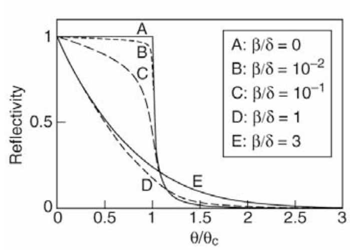

- finite β/δ rounds the sharp angular dependence
- cutoff angle and absorption edges can enhance the sharpness
- note the effects of oxide layers and surface contamination

. . . for real materials

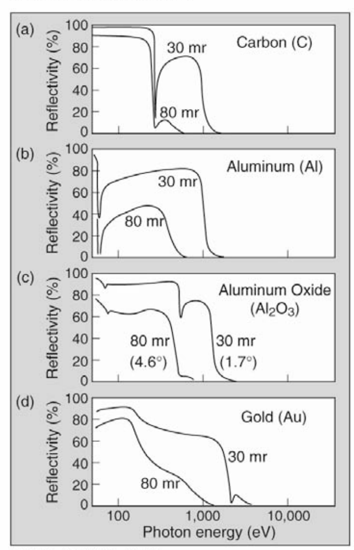

(Henke, Gullikson, Davis)

Ch03_TotalExtrnlReflc3.a

CheironSchool_Sept2011_Lec1.ppt 30

Normal incidence reflection at an interface

$$R_s = \frac{\left|\cos\phi - \sqrt{n^2 - \sin^2\phi}\right|^2}{\left|\cos\phi + \sqrt{n^2 - \sin^2\phi}\right|^2} \qquad (3.49)$$

at $\phi = 0$:

$$R_{s,\perp} = \frac{|1-n|^2}{|1+n|^2} = \frac{(1-n)(1-n^*)}{(1+n)(1+n^*)}$$

For $n = 1 - \delta + i\beta$

$$R_{s,\perp} = \frac{(\delta - i\beta)(\delta + i\beta)}{(2 - \delta + i\beta)(2 - \delta - i\beta)} = \frac{\delta^2 + \beta^2}{(2-\delta)^2 + \beta^2}$$

Reflectivity for x-ray and EUV radiation at normal incidence ($\phi = 0$):

$$\boxed{R_{s,\perp} \simeq \frac{\delta^2 + \beta^2}{4}} \qquad (3.50)$$

Example: Nickel @ 300 eV (4.13 nm)
$f_1^\circ = 17.8$ $f_2^\circ = 7.70$
$\delta = 0.0124$ $\beta = 0.00538$
$\Big\}\; R_\perp = 4.58 \times 10^{-5}$

Ch03_NormIncidReflc_5.05.ai

CheironSchool_Sept2011_Lec1.ppt 31

Focusing with curved glancing incidence optics

The Kirkpatrick-Baez mirror system

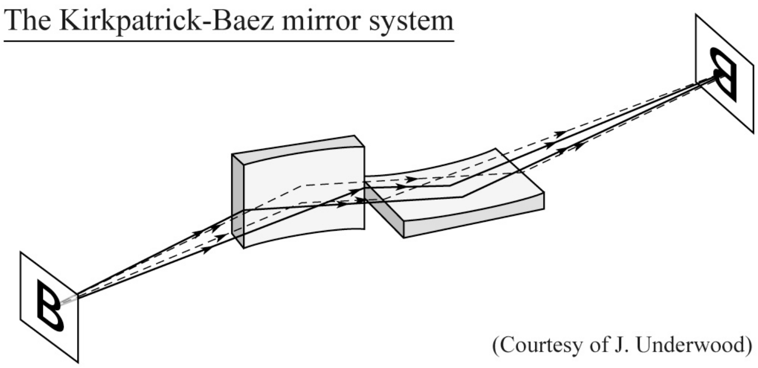

(Courtesy of J. Underwood)

- Two crossed cylinders (or ellipses)
- Astigmatism cancels
- Common use in synchrotron radiation beamlines
- Hard x-ray microprobe

Ch03_FocusCurv_Sept2010.ai

CheironSchool_Sept2011_Lec1.ppt 32

Fluorescent microprobe based in crossed cylinders

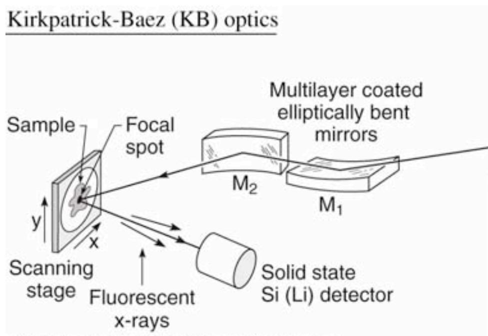

(Courtesy of A. Thompson and J. Underwood, LBNL; and R. Holm, Miles Lab)

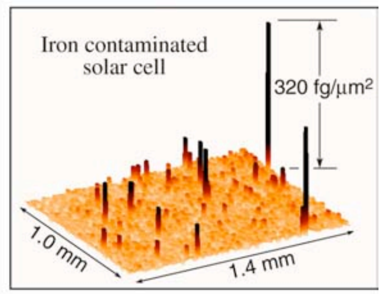

- Crossed cylinders at glancing incidence
- Ellipses better
- Photon in / photon out, low noise background
- Femtogram and part per billion (ppb) sensitivity
- Sub-micron focus (to 0.1 μm recently), but scattering gives several micron "50% encircled energy"
- K-B optics have many applications to synchrotron beamlines, fusion diagnostics, etc.

FluoresMicroprobe.ai

CheironSchool_Sept2011_Lec1.ppt 33

High resolution x-ray diffraction under high pressure using multilayer coated focusing optics

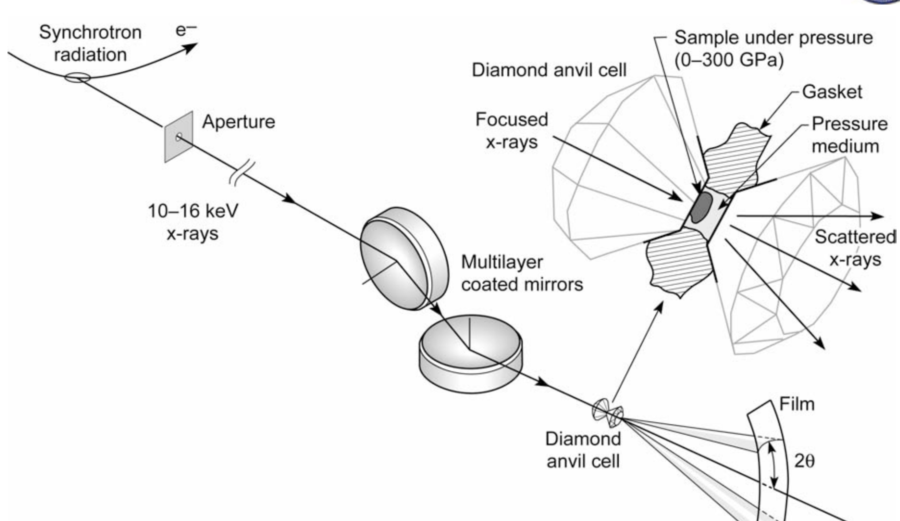

H.K. Mao et al., Science 277, 1220 (29 Aug. 1997)
Nature 396, 741 (24 Dec. 1998)

Ch04_F16aVG.ai

CheironSchool_Sept2011_Lec1.ppt 34

X-ray microprobe at SPring-8

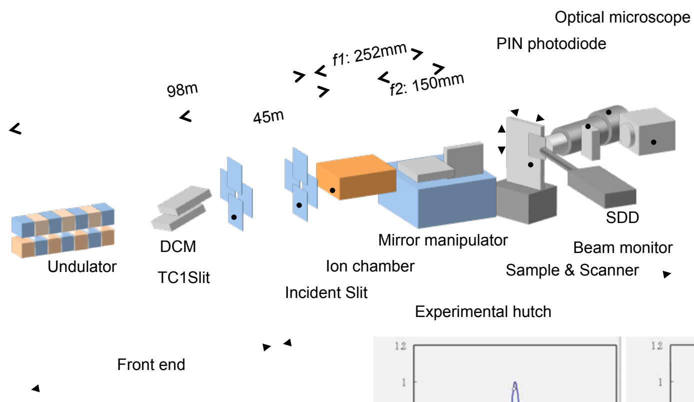

2006

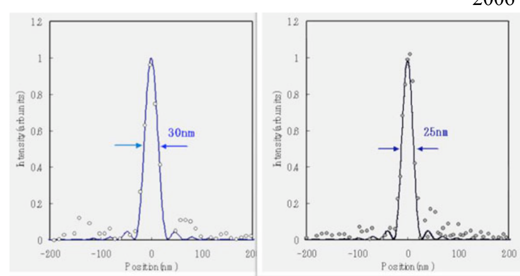

Courtesy of K. Yamauchi and
H. Mimura, Osaka University.

A high quality Mo/Si multilayer mirror

N = 40
d = 6.7

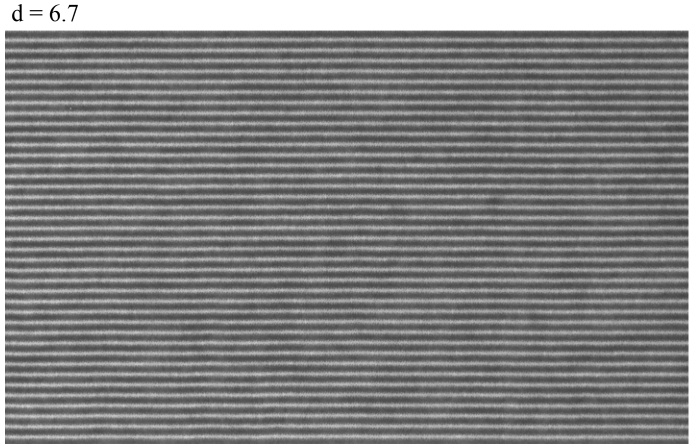

Courtesy of Saša Bajt (LLNL)

Scattering by density variations within a multilayer coating

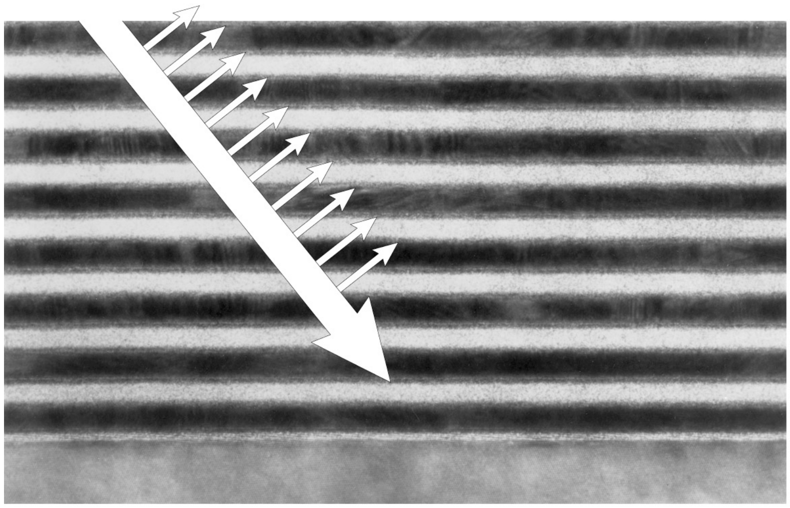

(T. Nguyen, CXRO/LBNL)

Ch04_F01_Feb2007.ai

CheironSchool_Sept2011_Lec1.ppt 37

Multilayer mirrors satisfy the Bragg condition

$$m\lambda = 2d \sin\theta$$

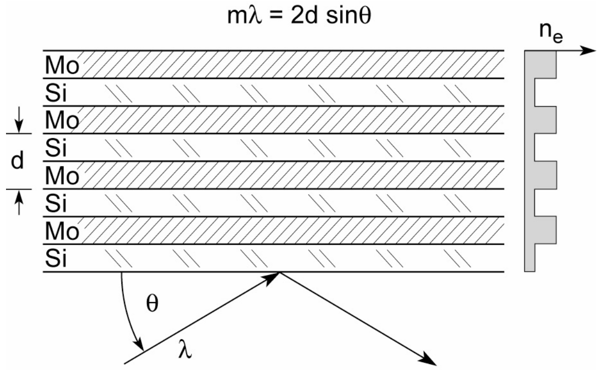

For normal incidence, $\theta = \pi/2$, first order ($m = 1$) reflection

$$\lambda = 2d$$

$$d = \lambda/2$$

if the two layers are approximately equal

$$\Delta t \simeq \lambda/4$$

a quarter-wave plate coating.

Ch04_MltlyrMirBragg1.ai

CheironSchool_Sept2011_Lec1.ppt 38

Multilayer mirrors satisfy the Bragg condition

$$m\lambda = 2d \sin\theta \left(1 - \frac{4\bar{\delta}d^2}{m^2\lambda^2}\right)$$

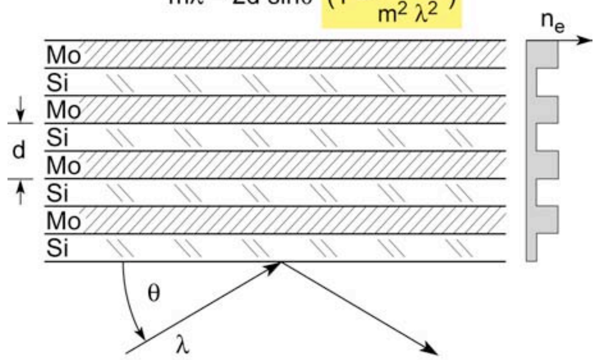

For normal incidence, $\theta = \pi/2$, first order ($m = 1$) reflection
$\lambda = 2d$
$d = \lambda/2$
if the two layers are approximately equal
$\Delta t \simeq \lambda/4$
a quarter-wave plate coating.

Ch04_MltlyrMirBragg2.ai

High reflectivity, thermally and environmentally robust multilayer coatings for high throughput EUV lithography

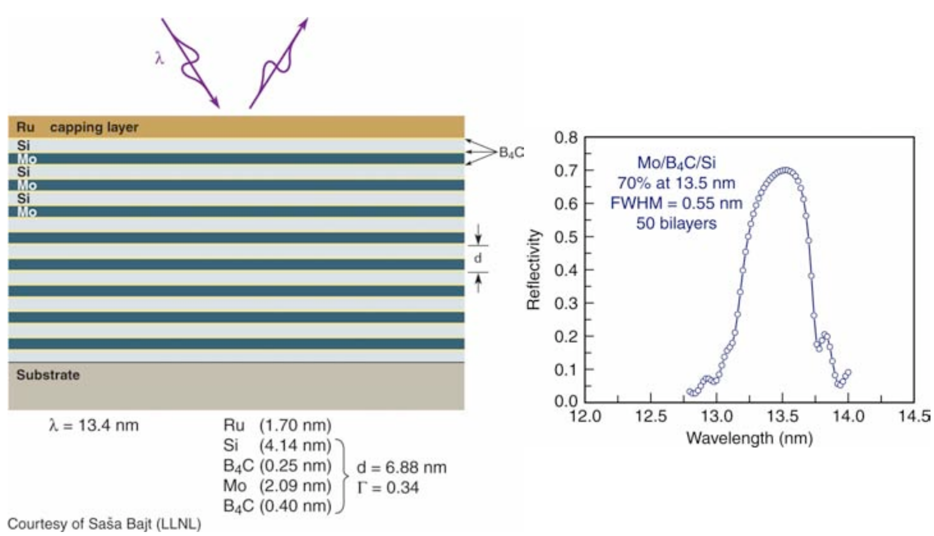

Atomic scattering factors for silicon (Z = 14)

σ_a(barns/atom) = μ(cm^2/g) × 46.64
E(keV)μ(cm^2/g) = f_2^0 × 1498.22

Silicon (Si)
Z = 14
Atomic weight = 28.086

Energy (eV)	f_1^0	f_2^0	μ(cm^2/g)
30	3.799	3.734E–01	1.865E+04
70	2.448	5.701E–01	1.220E+04
100	–5.657	4.580E+00	6.862E+04
300	12.00	6.439E+00	3.216E+04
700	13.31	1.951E+00	4.175E+03
1000	13.00	1.070E+00	1.602E+03
3000	14.23	1.961E+00	9.792E+02
7000	14.33	4.240E–01	9.075E+01
10000	14.28	2.135E–01	3.199E+01
30000	14.02	2.285E–02	1.141E+00

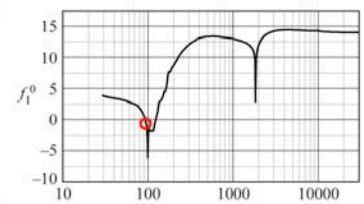

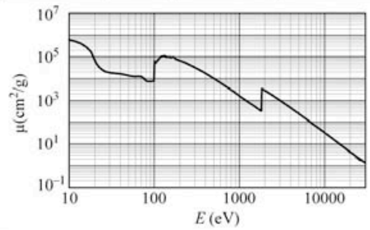

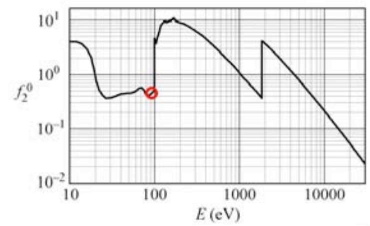

Edge Energies: K 1838.9 eV L_1 149.7 eV, L_2 99.8 eV, L_3 99.2 eV

(Henke and Gullikson; www-cxro.LBL.gov)

Ch02ApC_Tb1F07_Sept05.ai

CheironSchool_Sept2011_Lec1.ppt 41

Atomic scattering factors for molybdenum (Z = 42)

σ_a(barns/atom) = μ(cm^2/g) × 159.31
E(keV)μ(cm^2/g) = f_2^0 × 438.59

Molybdenum (Mo)
Z = 42
Atomic weight = 95.940

Energy (eV)	f_1^0	f_2^0	μ(cm^2/g)
30	1.071	5.292E+00	7.736E+04
70	19.38	4.732E+00	2.965E+04
100	14.02	1.124E+00	4.931E+03
300	4.609	1.568E+01	2.292E+04
700	31.41	1.819E+01	1.140E+04
1000	35.15	1.188E+01	5.210E+03
3000	35.88	1.366E+01	1.997E+03
7000	42.11	3.493E+00	2.189E+02
10000	41.67	1.881E+00	8.248E+01
30000	42.04	1.894E+00	2.769E+01

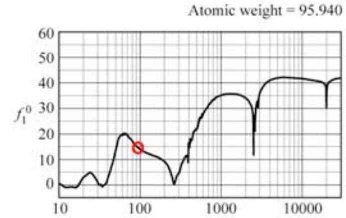

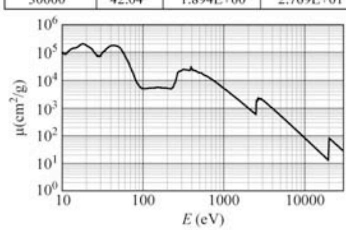

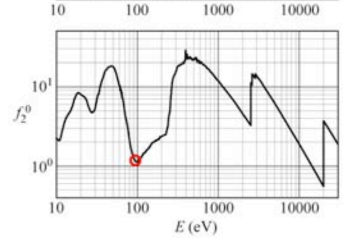

Edge Energies: K 19999.5 eV L_1 2865.5 eV, L_2 2625.1 eV, L_3 2520.2 eV M_1 506.3 eV, M_2 411.6 eV, M_3 394.0 eV, M_4 231.1 eV, M_5 227.9 eV N_1 63.2 eV, N_2 37.6 eV, N_3 35.5 eV

(Henke and Gullikson; www-cxro.LBL.gov)

Ch02ApC_Tb1F12_June2008.ai

CheironSchool_Sept2011_Lec1.ppt 42

CXRO Web Site

X-Ray Interactions with Matter . Search CXRO

- Facilities
- Publications
- Research
- X-Ray Tools
- Visitors
- Personnel
- Comments?
- Server Stats

www.cxro.LBL.gov/

- Atomic scattering factors
- EUV/x-ray properties of the elements
- Index of refraction for compound materials
- Absorption, attenuation lengths, transmission
- EUV/x-ray reflectivity (mirrors, thin films, multilayers)
- Transmission grating efficiencies
- Multilayer mirror achievements
- Other

CheironSchool_Sept2011_Lec1.ppt 43

Sputtered deposition of a multilayer coating

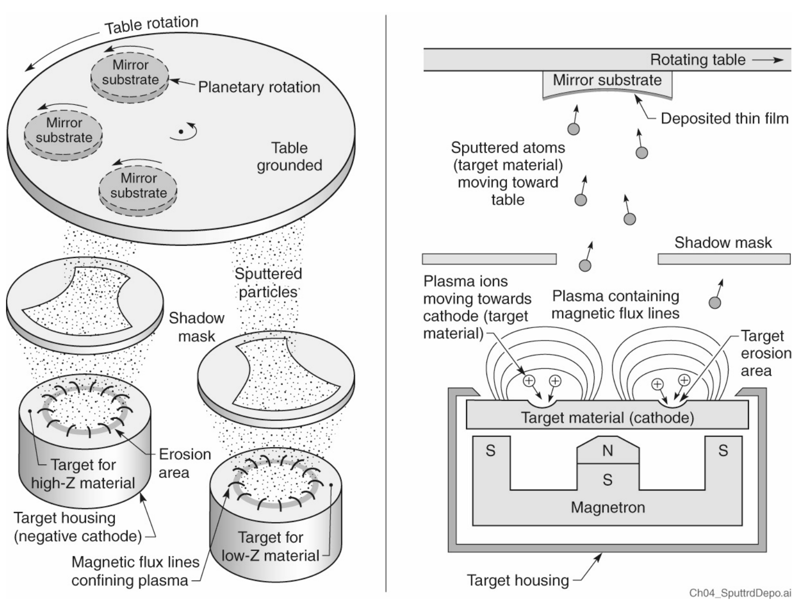

CheironSchool_Sept2011_Lec1.ppt 44

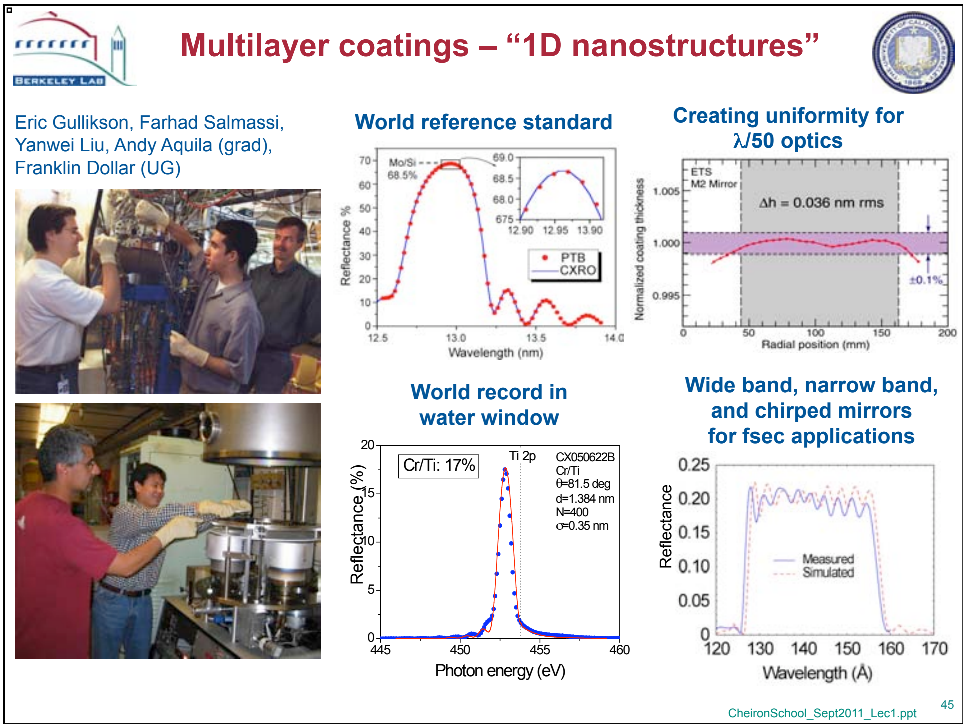
BERKELEY LAB
Multilayer coatings – "1D nanostructures"
Eric Gullikson, Farhad Salmassi,
Yanwei Liu, Andy Aquila (grad),
Franklin Dollar (UG)
World reference standard
Mo/Si
68.5%
Reflectance %
Wavelength (nm)
PTB
CXRO
Creating uniformity for
λ/50 optics
ETS
M2 Mirror
Δh = 0.036 nm rms
Normalized coating thickness
±0.1%
Radial position (mm)
World record in
water window
Cr/Ti: 17%
Ti 2p
CX050622B
Cr/Ti
θ=81.5 deg
d=1.384 nm
N=400
σ=0.35 nm
Reflectance (%)
Photon energy (eV)
Wide band, narrow band,
and chirped mirrors
for fsec applications
Reflectance
Measured
Simulated
Wavelength (Å)
CheironSchool_Sept2011_Lec1.ppt
45

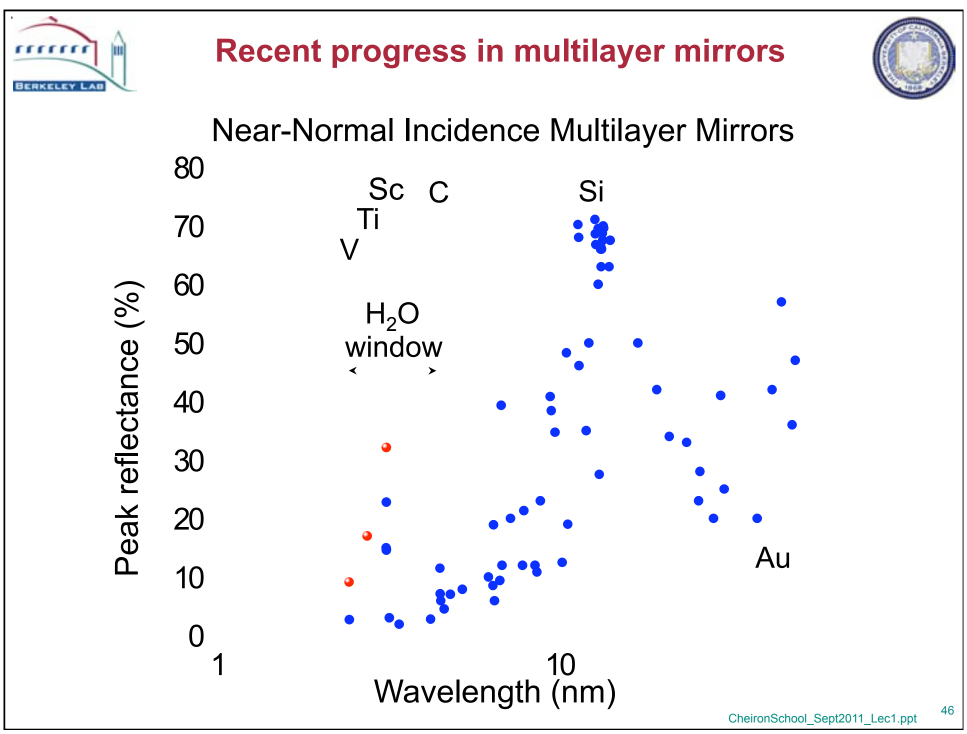
BERKELEY LAB
Recent progress in multilayer mirrors
Near-Normal Incidence Multilayer Mirrors
Peak reflectance (%)
Sc
C
Ti
V
Si
H2O
window
Au
Wavelength (nm)
CheironSchool_Sept2011_Lec1.ppt
46

Broad bandwidth mirrors needed for as/fs pulses

$\Delta E(\mathrm{eV}) \cdot \Delta\tau(\mathrm{fs}) \geq 1.8\ \mathrm{fs}\cdot\mathrm{eV}$ (FWHM)

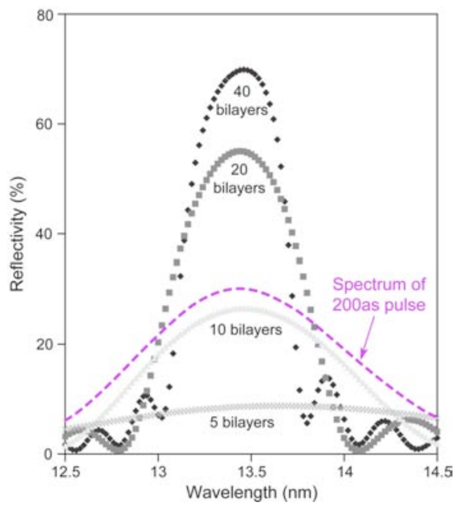

- Multilayer mirrors depend on constructive interference from individual interfaces
- Higher reflectivity needs more layers
- Bandwidth gets narrower with more layers

Attosecond pulse

→ Broad bandwidth

→ Limited number of layers

N<10 layers required for 200 as pulse (@13nm)

CheironSchool_Sept2011_Lec1.ppt 47

Aperiodic multilayers for asec application

Optimizing multilayers for specific applications requires the use of simulation of a multilayer stack with variations in the thickness of each material in the multilayer.

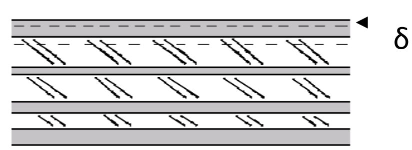

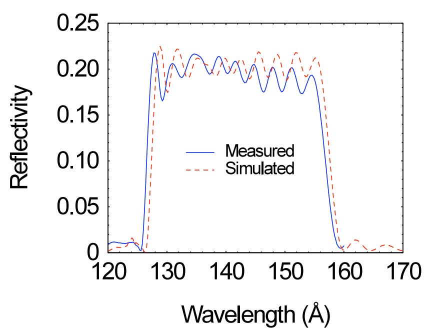

Successful design of aperiodic multilayers requires:

1. EM wave in multilayer structure
2. Optimization Algorithm
3. Sample preparation
4. Verification

A. L. Aquila, F. Salmassi, F. Dollar, Y. Liu, and E. Gullikson, "Developments in realistic design for aperiodic Mo/Si multilayer mirrors," Opt. Express ***14,*** *10073-10078 (2006)*

CheironSchool_Sept2011_Lec1.ppt 48

The Cassegrain Telescope with multilayer coatings for EUV imaging of the solar corona

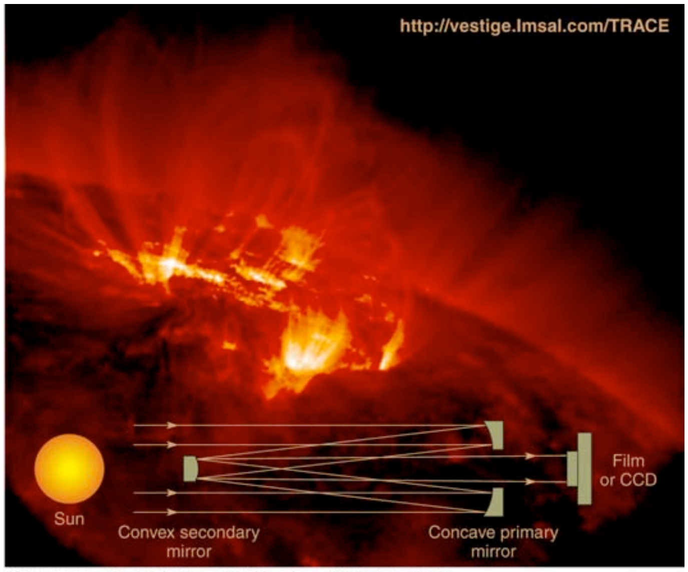

(Photo courtesy of L.Golub, Harvard-Smithsonian and T. Barbee, LLNL)

CheironSchool_Sept2011_Lec1.ppt 49

Multilayer Laue Lens for focusing hard x-rays

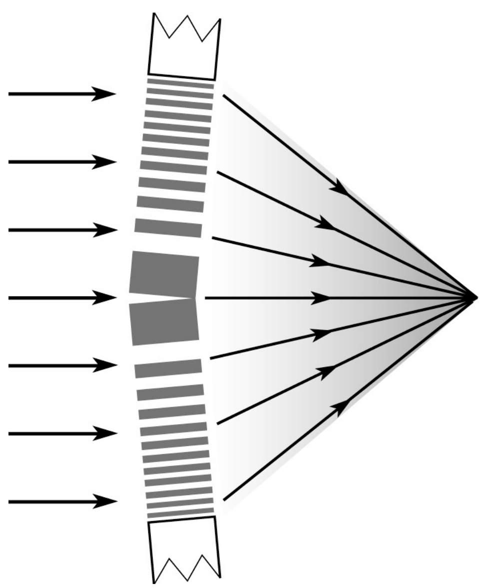

CheironSchool_Sept2011_Lec1.ppt 50

Photon energy, wavelength, power

$$\boxed{\hbar\omega \cdot \lambda = hc = 1239.842 \text{ eV nm}} \qquad (1.1)$$

$$\boxed{1 \text{ joule} \Rightarrow 5.034 \times 10^{15} \lambda[\text{nm}] \text{ photons}} \qquad (1.2a)$$

$$\boxed{1 \text{ watt} \Rightarrow 5.034 \times 10^{15} \lambda[\text{nm}] \frac{\text{photons}}{\text{s}}} \qquad (1.2b)$$

Ch01_Eqs1.1_2.ai

CheironSchool_Sept2011_Lec1.ppt 51

Lectures online at www.youtube.com

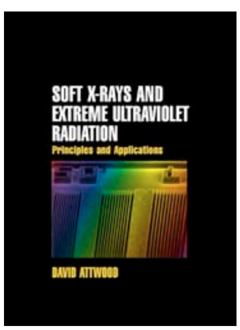

Amazon.com

UC Berkeley
www.coe.berkeley.edu/AST/sxreuv
www.coe.berkeley.edu/AST/srms
www.coe.berkeley.edu/AST/sxr2009

CheironSchool_Sept2011_Lec1.ppt 52